

RESEARCH

Open Access



Industrial dry spinning processes: algorithmic for a two-phase fiber model in airflows

Manuel Wieland¹, Walter Arne¹, Nicole Marheineke^{2*} and Raimund Wegener¹

*Correspondence:

marheineke@uni-trier.de

²Lehrstuhl Modellierung und Numerik, Universität Trier, Trier, Germany

Full list of author information is available at the end of the article

Abstract

The dry spinning of fibers can be described by three-dimensional multi-phase flow models that contain key effects like solvent evaporation and fiber-air interaction. Since the direct numerical simulation of the three-dimensional models is in general not possible, dimensionally reduced models are deduced. We recently developed a one-two-dimensional fiber model and presented a problem-tailored numerical solution strategy in Wieland et al. (*J Comput Phys* 384:326–348, 2019). However, in view of industrial setups with multiple fibers spun simultaneously the numerical schemes must be accelerated to achieve feasible simulation times. The bottleneck builds the computation of the radial concentration and temperature profiles as well as their cross-sectionally averaged values. In this paper we address this issue and develop efficient numerical algorithms.

MSC: 34B08; 68U20; 35Q79; 45D05; 76-XX

Keywords: Dry spinning; Fiber dynamics; Parametric boundary value problem; Homotopy method; Integral equations

1 Introduction

In dry spinning processes a polymer solvent mixture is extruded from multiple nozzles into a spinning duct with a tempered air stream. The air stream leads to evaporation of the solvent and leaves solidified fibers behind. At the bottom of the spinning duct the fibers are usually drawn down by a take up roller.

The dry spinning of fibers can be modeled by three-dimensional continuum mechanics. The fibers can be treated as two-phase media of two mutually-penetrating continua (polymer and solvent) interacting with a surrounding aerodynamic flow phase, [13]. However, governing the key effects, like solvent evaporation and interaction between multiple slender fibers and air [21], rises the computational complexity of the multiphase-multiscale problem such that the direct numerical simulation of the three-dimensional models is in general not possible. Therefore, several surrogate fiber models for dry spinning have been developed in the last decades. Starting from uni-axial stationary one-dimensional models based on cross-sectionally averaged balances in [14, 15], a two-dimensional model with concentration-dependent rheological laws covering the radial diffusion effects was

© The Author(s) 2020. This article is licensed under a Creative Commons Attribution 4.0 International License, which permits use, sharing, adaptation, distribution and reproduction in any medium or format, as long as you give appropriate credit to the original author(s) and the source, provide a link to the Creative Commons licence, and indicate if changes were made. The images or other third party material in this article are included in the article's Creative Commons licence, unless indicated otherwise in a credit line to the material. If material is not included in the article's Creative Commons licence and your intended use is not permitted by statutory regulation or exceeds the permitted use, you will need to obtain permission directly from the copyright holder. To view a copy of this licence, visit <http://creativecommons.org/licenses/by/4.0/>.

employed in [4]. A comparative theoretical and experimental study of a cellulose acetate/acetone dry spinning system was presented in [17]. The works of [8, 9] extended the models from viscous to viscoelastic material behavior. In [19] we recently developed a dimensionally reduced fiber model which consists of one-dimensional equations for tangential fiber velocity and stress and two-dimensional advection-diffusion equations covering the cross-sectional variations of polymer mass fraction and fiber temperature. We extended this uni-axial fiber model to curved fibers utilizing the theory of Cosserat rods in [20]. Due to the dimensional reduction, certain physical phenomena are certainly not shown by the surrogates. With our model, a description of the shark skin formation is for example not possible due to the neglect of radial velocity information, but the essential effect of solvent evaporation is correctly covered. In comparison to the referential solution of a three-dimensional model, the results are convincing, providing a good approximation, while drastically reducing the computational time, cf. [19]. The numerical solution framework proposed in [19] allows the incorporation of mutual fiber-air interaction in a two-way coupling and, hence, makes the simulation of industrial dry spinning feasible. The simulation results for a cellulose acetate/acetone dry spinning setup stand in accordance to the data in [17]. In view of process design and optimization of complex industrial setups with multiple hundred to more than one thousand fibers spun simultaneously, however, the numerical treatment is still too time-consuming. When solving the coupled one-two-dimensional problem iteratively, it turns out that the computation of the radial profiles of polymer mass fraction and fiber temperature as well as their associated cross-sectionally averaged values builds the bottleneck. In this paper, we address this computational challenge. We develop new algorithmic strategies that represent significant improvements on the existing state of the art. Based on a generalized problem description we give details for an efficient implementation of the underlying routines and demonstrate their performance for an industrial example.

The scientific novelty of this paper is the algorithmic; the model and the industrial example are taken from [19]. With regard to a closed presentation and independent readability, the paper is structured as follows. For a better understanding of the underlying multiscale-multiphase problem we start with the three-dimensional fiber description based on a mixture model ansatz in Sect. 2. The dimensionally reduced one-two-dimensional fiber model according to [19] is given in Sect. 3. The core of the paper is Sect. 4, where we introduce new numerical strategies for the computation of the two-dimensional profiles and averaged quantities. Moreover, based on a general problem formulation we describe the coupling concept for the solution of the underlying one-two-dimensional problem and give details for its implementation in view of efficient simulations. In Sect. 5 we apply the framework to the industrial dry spinning of a cellulose acetate-acetone mixture in air. Investigating the computational performance, we discuss the improvements of our developed numerical schemes compared to [19].

2 Underlying three-dimensional multiphase-multiscale problem

For a better understanding of the dimensionally reduced one-two-dimensional fiber model given in [19], we describe the underlying (Euler-)stationary three-dimensional dry spinning model for a single viscous uni-axial fiber in a surrounding airflow in this section. Since in dry spinning processes no relevant transient effects occur, we restrict to a steady consideration. Let $\mathcal{D} \subset \mathbb{R}^3$ be the a priori unknown fiber domain whose boundary $\partial\mathcal{D} = \Gamma_{\text{in}} \cup \Gamma_{\text{fr}} \cup \Gamma_{\text{out}}$ consists of the fixed inlet at the nozzle Γ_{in} , the free lateral fiber

surface Γ_{fr} and the outlet Γ_{out} . Proceeding from balance laws for mass, momentum and energy for the two phases i in \mathcal{D} , $i \in \{p, d\}$ (polymer and diluent) [13], we employ the mixture model ansatz of [11] to reduce the balances for momentum and energy for the single phases to balances for the mixture. The quantities for the single phases are indicated by the respective index i , $i \in \{p, d\}$. Note that throughout this paper we use the terms ‘diluent’ and ‘solvent’ synonymously.

Let ρ_i [kg/m³] and \mathbf{v}_i [m/s] be the partial densities and velocities for the polymer and diluent phases as well as h_i [J/kg] the partial specific enthalpies of polymer and diluent in the mixture, $i \in \{p, d\}$. Assuming an Eulerian (spatial) description, the stationary mass, momentum and energy balances for the two phases are modeled as

$$\nabla \cdot (\rho_i \mathbf{v}_i) = 0, \quad i \in \{p, d\}, \tag{1a}$$

$$\nabla \cdot (\rho_i \mathbf{v}_i \otimes \mathbf{v}_i) = \nabla \cdot \boldsymbol{\Sigma}_i^T + \mathbf{f}_i, \quad i \in \{p, d\}, \tag{1b}$$

$$\nabla \cdot (\rho h_i \mathbf{v}_i) = \nabla \cdot (C_i \nabla T), \quad i \in \{p, d\}, \tag{1c}$$

with respective stress tensors $\boldsymbol{\Sigma}_i$ [Pa] and body force densities \mathbf{f}_i [N/m³] acting on phase i . In the energy balances (1c), ρ [kg/m³] denotes the density of the mixture and the right hand sides represent the energy transport by heat conduction at mixture temperature T [K] and thermal conductivities C_i [W/(m K)]. Effects of inner friction, convective terms due to pressure fluctuations as well as energy transfer caused by body forces are neglected.

The mixture model ansatz according to [11] treats the two phases as interpenetrable continua. Its idea is to consider only one momentum equation as sum of the phase balances (1b) and only one energy balance equation as sum of (1c). The mixture density ρ , mixture stress tensor $\boldsymbol{\Sigma}$, total body force \mathbf{f} , mixture specific enthalpy h as well as the mixture thermal conductivity C are the sums of the quantities of the single phases, i.e.,

$$k = k_p + k_d, \quad k \in \{\rho, \boldsymbol{\Sigma}, \mathbf{f}, h, C\}.$$

For the mixture we assume ideality, i.e., the volume does not change under mixing and the enthalpy of mixing is zero. This leads to the relations

$$1 = \frac{\rho_p}{\rho_p^0} + \frac{\rho_d}{\rho_d^0}, \quad \rho h_i = \rho_i h_i^0, \quad i \in \{p, d\},$$

where ρ_i^0 , h_i^0 denote the material densities and specific enthalpies of pure polymer and solvent. These material parameters might be specified depending on the temperature. Together with the definition of the mixture specific enthalpy h the relation for the enthalpies results in the more common expression

$$h = \frac{\rho_p}{\rho} h_p^0 + \frac{\rho_d}{\rho} h_d^0.$$

The temperature derivatives of h_p^0 , h_d^0 and h are in particular the specific heat capacities q_p^0 , q_d^0 and q [J/(kg K)] for constant pressure, yielding

$$q = \frac{\rho_p}{\rho} q_p^0 + \frac{\rho_d}{\rho} q_d^0.$$

Here, we used the fact that the mass fractions of the single phases do not explicitly depend on the temperature, i.e., $\partial_T(\rho_i/\rho) = 0$, $i \in \{p, d\}$. For the stress tensor Σ we assume incompressibility and a Newtonian fluid with dynamic mixture viscosity μ [Pa s], i.e., $\Sigma = -p\mathbf{I} + \mu(\nabla\mathbf{v} + (\nabla\mathbf{v})^T)$ with mixture pressure p [Pa], mixture velocity \mathbf{v} [m/s] and $\mathbf{I} \in \mathbb{R}^{3 \times 3}$ denoting the identity matrix. The definition of the mixture velocity \mathbf{v} requires a special treatment: Since the intended consideration of only one momentum balance does not close our model, we have to employ constitutive relations for the differences between the phase velocities and the mixture velocity. In our dry spinning scenario we consider the polymer phase as dominating phase and the diluent phase as secondary phase. Therefore, we fix the polymer velocity as mixture velocity, i.e., $\mathbf{v} = \mathbf{v}_p$. Then, only one constitutive relation for the difference between the mixture velocity and the diluent velocity $\mathbf{v}_{pd} = \mathbf{v} - \mathbf{v}_d$ is needed. We use Fick's law in a version, which is linear with respect to the diluent mass fraction ρ_d/ρ , namely $\rho_d\mathbf{v}_{pd} = \rho D \nabla(\rho_d/\rho)$, with D [m²/s] denoting the diffusion coefficient of the diluent in the polymer. This formulation is appropriate to obtain an efficiently evaluable linear advection-diffusion equation for the polymer mass fraction in the dimensionally reduced fiber model (cf. Sect. 3). Employing $\mathbf{v} = \mathbf{v}_p$ and Fick's law the mass balances for polymer and diluent (1a) become

$$\nabla \cdot (\rho_p \mathbf{v}) = 0, \quad \nabla \cdot (\rho_d \mathbf{v}) - \nabla \cdot \left(\rho D \nabla \left(\frac{\rho_d}{\rho} \right) \right) = 0.$$

Moreover, summing up the momentum phase balances (1b) and neglecting diffusive parts in the stresses yields the mixture momentum balance

$$\nabla \cdot (\rho \mathbf{v} \otimes \mathbf{v}) - \nabla \cdot \left(\rho D \left(\mathbf{v} \otimes \nabla \left(\frac{\rho_d}{\rho} \right) + \nabla \left(\frac{\rho_d}{\rho} \right) \otimes \mathbf{v} \right) \right) = \nabla \cdot \Sigma^T + \mathbf{f}.$$

Analogously using Fick's law and the phase balances (1c) we obtain the total energy balance for the mixture

$$\nabla \cdot (\rho h \mathbf{v}) - \nabla \cdot \left(h_d^0 \rho D \nabla \left(\frac{\rho_d}{\rho} \right) \right) = \nabla \cdot (C \nabla T).$$

Introducing appropriate boundary conditions, the stationary free boundary value problem (BVP) for the fiber unknowns ρ_p, p, \mathbf{v}, T and \mathcal{D} is given by

System 1 (Three-dimensional free BVP) *Balance laws in \mathcal{D} :*

$$\begin{aligned} \nabla \cdot (\rho_p \mathbf{v}) &= 0, \\ \nabla \cdot (\rho_d \mathbf{v}) &= \nabla \cdot \left(\rho D \nabla \left(\frac{\rho_d}{\rho} \right) \right), \\ \nabla \cdot (\rho \mathbf{v} \otimes \mathbf{v}) - \nabla \cdot \left(\rho D \left(\mathbf{v} \otimes \nabla \left(\frac{\rho_d}{\rho} \right) + \nabla \left(\frac{\rho_d}{\rho} \right) \otimes \mathbf{v} \right) \right) &= \nabla \cdot \Sigma^T + \mathbf{f}, \\ \nabla \cdot (\rho h \mathbf{v}) - \nabla \cdot \left(h_d^0 \rho D \nabla \left(\frac{\rho_d}{\rho} \right) \right) &= \nabla \cdot (C \nabla T). \end{aligned}$$

Kinematic, dynamic, mass and heat flux respective boundary conditions on Γ_{fr} :

$$\mathbf{v} \cdot \mathbf{n} = 0,$$

$$\begin{aligned} \Sigma \cdot \mathbf{n} &= \mathbf{f}_*, \\ -\rho D \nabla \left(\frac{\rho_d}{\rho} \right) \cdot \mathbf{n} &= j_c, \quad j_c = \gamma \left(\frac{\rho_d}{\rho} - \frac{\rho_{d,*}}{\varrho_*} \right), \\ -C \nabla T \cdot \mathbf{n} &= j_T + j_c (\delta - h_d^0), \quad j_T = \alpha (T - T_*). \end{aligned}$$

Inlet boundary conditions on Γ_{in} :

$$\mathbf{v} = \mathbf{v}_{in}, \quad \rho_d = \rho_{d,in}, \quad T = T_{in}.$$

Outlet boundary condition on Γ_{out} :

$$\mathbf{v} = \mathbf{v}_{out}.$$

Constitutive laws:

$$1 = \frac{\rho_p}{\rho_p^0} + \frac{\rho_d}{\rho_d^0}, \quad h = \frac{\rho_p}{\rho} h_p^0 + \frac{\rho_d}{\rho} h_d^0, \quad \Sigma = -p \mathbf{I} + \mu (\nabla \mathbf{v} + (\nabla \mathbf{v})^T).$$

Here, we consider body forces due to gravity, i.e., $\mathbf{f} = \rho \mathbf{g}$, as well as surface forces \mathbf{f}_* [Pa] due to the surrounding airflow. The geometry is specified via the kinematic boundary condition on Γ_{fr} with unit outer normal vector \mathbf{n} . At the lateral fiber surface the diluent density has a jump due to the solvent evaporation, moreover, it changes rapidly in the boundary layer that the surrounding air forms around the fiber. The diluent mass flux j_c [kg/(m²s)] in the aerodynamic boundary layer can be modeled by the difference of the diluent density in the air at the fiber surface ς_* [kg/m³] and away from the fiber $\rho_{d,*}$ [kg/m³] with convective mass transfer coefficient β [m/s], i.e., $j_c = \beta (\varsigma_* - \rho_{d,*})$. Let $c = \rho_p / \rho = 1 - \rho_d / \rho$ be the polymer mass fraction, then we particularly use a formulation for j_c in terms of the mass fraction associated transfer coefficient $\gamma = \beta \varrho_*$ [kg/(m²s)] with $\varrho_* = \varsigma_* \rho / \rho_d$ [kg/m³] in System 1. The temperature is continuous at the fiber surface, whereas the heat flux has a jump because of the heat exchange in the air due to the solvent evaporation with evaporation enthalpy δ [J/kg] of the diluent. In the aerodynamic boundary layer the heat flux j_T [W/m²] is described— analogously to the mass flux—by the difference of the temperature at the fiber surface and away from the fiber T_* [K] with heat transfer coefficient α [W/(m²K)]. The parameters δ and ς_* might be functions of c and T , whereas the transfer coefficients α and β depend on the state of the surrounding airflow and especially on the relative velocity between fiber and airflow. In System 1 the surrounding airflow is assumed to be known in the sense that the quantities \mathbf{f}_* , $\rho_{d,*}$ and T_* as well as the airflow dependencies of α and β are given for each point of the fiber surface. Moreover, the parameters D , C and μ might depend on the mass fraction c and temperature T with suitable models assumed to be available.

Remark 1 (Mass transfer) The used formulation of the diluent mass transfer j_c is motivated from the fact that at the fiber surface the diluent density in the air is mainly linearly proportional to the diluent density in the fiber, i.e., $\varsigma_* \sim \rho_d$. Setting $\varsigma_* = (\rho_d / \rho) \varrho_*$ separates the linear part from the remainder ϱ_* . The mass transfer is principally driven from the linear part in terms of a Robin-type boundary condition, whereas the remainder ϱ_*

is incorporated in the transfer coefficient $\gamma = \beta \varrho_*$. This splitting might allow a different treatment of the terms, which becomes essentially for our numerical treatment of the problem.

3 Reduced fiber dry spinning model

Due to the complexity of the three-dimensional problem (System 1) that prevents the simulations of industrial dry spinning setups, we proposed a dimensionally reduced model in [19] that is of good approximation quality and efficiently evaluable. It combines the relevant two-dimensional aspects (radial profiles for polymer mass fraction c and temperature T), that are essential due to the evaporation of solvent [14, 15], with one-dimensional cross-sectionally averaged balances for tangential fiber velocity u and stress σ . In dimensionless form the model for u, σ, c, T is given by

System 2 (One-two-dimensional BVP) *Cross-sectionally averaged balance laws, $s \in (0, 1)$:*

$$\begin{aligned} L^{-1} \partial_s u &= \text{Re} \frac{1}{3 \langle \mu(c, T) \rangle_{R^2}} \sigma, \\ L^{-1} \partial_s \sigma &= \text{Re} \frac{Q}{\bar{c}} \frac{1}{3 \langle \mu(c, T) \rangle_{R^2}} \sigma - \frac{1}{\text{Fr}^2} \frac{Q}{\bar{c}} \frac{1}{u} - f_{\text{air}}, \end{aligned} \tag{2a}$$

with boundary conditions at inlet $s = 0$ and outlet $s = 1$:

$$u(0) = u_{\text{in}}, \quad u(1) = \text{Dr} u_{\text{out}}.$$

Radial equations, $(r, s) \in (0, 1)^2$:

$$\begin{aligned} L^{-1} u \partial_s c - \frac{1}{\varepsilon \text{Pe}_c} \frac{\bar{c} D(\bar{c}, \bar{T})}{R^2 r} \partial_r (r \partial_r c) &= 0, \\ L^{-1} \rho(\bar{c}, \bar{T}) q(\bar{c}, \bar{T}) u \partial_s T - \frac{1}{\varepsilon \text{Pe}_T} \frac{C(\bar{c}, \bar{T})}{R^2 r} \partial_r (r \partial_r T) &= 0, \end{aligned} \tag{2b}$$

with boundary conditions at inlet $s = 0$, fiber surface $r = 1$ and symmetry boundary $r = 0$:

$$\begin{aligned} c|_{s=0} &= c_{\text{in}}, \quad \partial_r c|_{r=0} = 0, \\ \frac{1}{\text{Pe}_c} \frac{\rho(\bar{c}, \bar{T}) D(\bar{c}, \bar{T})}{R} \partial_r c|_{r=1} &= \text{St}_{jc}(c, T)|_{r=1}, \\ T|_{s=0} &= T_{\text{in}}, \quad \partial_r T|_{r=1} = 0, \\ -\frac{1}{\text{Pe}_T} \frac{C(\bar{c}, \bar{T})}{R} \partial_r T|_{r=1} &= (\text{St}_T j_T(T) + \text{St}_{jc}(c, T) (\delta(T) - h_d^0(T)))|_{r=1}, \\ j_c(c, T) &= -\gamma(c, T)(c - c_{\text{ref}}(c, T)), \quad j_T(T) = \alpha(T - T_*). \end{aligned}$$

Constitutive laws and geometric relation:

$$\begin{aligned} \rho^{-1}(c, T) &= c(\rho_p^0)^{-1}(T) + (1 - c)(\rho_d^0)^{-1}(T), \quad q_d^0(T) = \partial_T h_d^0(T), \\ q(c, T) &= c q_p^0(T) + (1 - c) q_d^0(T), \quad R(s) = \sqrt{\frac{Q}{\pi(\bar{c} \rho(\bar{c}, \bar{T}) u)|_s}}. \end{aligned}$$

Abbreviations:

$$\bar{c} = \frac{1}{\pi R^2} \langle c \rangle_{R^2}, \quad \bar{T} = \frac{1}{\pi R^2} \langle T \rangle_{R^2}, \quad \langle y \rangle_{R^2(s)} = 2\pi R^2(s) \int_0^1 y(r, s) r dr,$$

$$Q = c_{in} \rho_{in} u_{in} R_{in}^2 \pi.$$

The one-dimensional equations for the tangential fiber velocity u and stress σ result from averaging the Newtonian stress tensor Σ and the momentum balance in System 1 over circular fiber cross-sections. The two-dimensional advection-diffusion equations for the polymer mass fraction c and temperature T , which reveal the radial effects that are essential due to evaporation, are obtained from the diluent mass and energy balance in System 1 by the assumption of radial symmetry and by linearization around the cross-sectional averaged polymer mass fraction \bar{c} and temperature \bar{T} . Moreover, averaging the polymer mass balance in System 1 over the fiber cross-sections yields the constant polymer mass flux $Q = \bar{c} \rho(\bar{c}, \bar{T}) u R^2 \pi = c_{in} \rho(c_{in}, T_{in}) u_{in} R_{in}^2 \pi$. This means we do not face a free boundary value problem anymore, but can conclude the fiber radius R from the boundary conditions at the inlet. For further details see [19].

Remark 2 (Non-dimensionalization and scaling) System 2 is formulated with respect to dimensionless quantities y that have been scaled onto the space domain $(0, 1)$ (one-dimensional quantities) and $(0, 1)^2$ (two-dimensional quantities), respectively. The non-dimensionalization and scaling are done in separate steps. First, dimensionless quantities are introduced as

$$\tilde{y}(\tilde{s}) = \check{y}(s_0 \tilde{s}) / y_0, \quad \tilde{y}(\tilde{r}, \tilde{s}) = \check{y}(d_0 \tilde{r}, s_0 \tilde{s}) / y_0$$

for any scalar- or vector-valued dimensionful quantity \check{y} and corresponding reference value y_0 . Due to technical reasons we use slightly different scales compared to [19], for the reference values and resulting dimensionless numbers see Table 1. After non-dimensionalization the equations are considered on the non-dimensional space domain

Table 1 Overview over composite reference values used for non-dimensionalization of the uni-axial fiber dry spinning model and the resulting dimensionless numbers. Here, the scales $Q_{M,0}, v_0, r_0, d_0, \mu_0, q_0, T_0, \alpha_0, \gamma_0, C_0, D_0, u_{out,0}, \rho_{*,0}, p_{*,0}, q_{*,0}, v_{*,0}, \lambda_{*,0}, D_{d,*,0}$ are assumed to be given from the considered setup

Composite reference values			Dimensionless numbers	
Description	Formula	Unit	Description	Formula
Length scale	$s_0 = r_0$	m	Slenderness	$\varepsilon = d_0 / r_0$
Fiber length	$L_0 = r_0$	m	Reynolds	$Re = Q_{M,0} v_0 r_0 / (d_0^2 \mu_0)$
Cross-sectional radius	$R_0 = d_0$	m	Froude	$Fr = v_0 / \sqrt{g r_0}$
Mass density	$\rho_0 = Q_{M,0} / d_0^2$	kg/m ³	Drawing	$Dr = u_{out,0} / u_0$
Scalar velocity	$u_0 = v_0$	m/s	Mass Peclet	$Pe_c = v_0 d_0 / D_0$
Stress	$\sigma_0 = Q_{M,0} v_0^2$	N	Temperature Peclet	$Pe_T = Q_{M,0} v_0 q_0 / (C_0 d_0)$
Outer force	$f_0 = Q_{M,0} v_0^2 / r_0$	N/m	Mass Stanton	$St_c = \gamma_0 d_0^2 / (v_0 Q_{M,0})$
Enthalpy	$h_0 = q_0 T_0$	J/kg	Temperature Stanton	$St_T = \alpha_0 d_0^2 / (v_0 Q_{M,0} q_0)$
Evaporation enthalpy	$\delta_0 = h_0$	J/kg	Air-fiber Reynolds	$Re_* = d_0 v_0 / \nu_{*,0}$
Mass transfer coefficient	$\beta_0 = \gamma_0 / \rho_{*,0}$	m/s	Nusselt	$Nu_* = \alpha_0 d_0 / \lambda_{*,0}$
Air temperature	$T_{*,0} = T_0$	K	Prandtl	$Pr_* = q_{*,0} \rho_{*,0} \nu_{*,0} / \lambda_{*,0}$
Air velocity	$v_{*,0} = v_0$	m/s	Sherwood	$Sh_* = \gamma_0 d_0 / (\rho_{*,0} D_{d,*,0})$
			Schmidt	$Sc_* = \nu_{*,0} / D_{d,*,0}$

$(0, L)$ (one-dimensional equations) and $(0, R(\tilde{s})) \times (0, L)$ (two-dimensional equations), respectively. Second, to simplify the numerical treatment of the equations, one-dimensional equations are transformed onto the space domain $(0, 1)$ and two-dimensional equations onto the space domain $(0, 1)^2$ via

$$y(s) = \tilde{y}(Ls), \quad y(r, s) = \tilde{y}(R(Ls)r, Ls),$$

respectively. Since the fiber radius R is an a priori unknown, this domain transformation omits domain changes during the numerical solution of the problem, which would cause computational expensive re-meshing of the computational domain. The transformation inserts the unknown R into our model equations, but this can efficiently be handled with our numerical solution algorithm. Since the dimensionful fiber length \check{L} is a priori known, choosing $s_0 = r_0 = \check{L}$ would lead to a fiber length equal to one in non-dimensional form (i.e., $L = 1$).

Remark 3 (Averaged viscosity) In System 2 we could approximate the cross-sectionally averaged dynamic viscosity in the same way as the densities, i.e.,

$$\langle \mu(c, T) \rangle_{R^2} / (\pi R^2) \approx \mu(\bar{c}, \bar{T}).$$

However, due to in general highly nonlinear rheological models for the dynamic viscosity, this approximation is not feasible for industrial setups.

As aerodynamic force model f_{air} we use

$$f_{\text{air}} = \frac{A_\star}{\text{Re}_\star^2} \frac{\rho_\star v_\star^2}{2R} \mathbf{F} \left(\boldsymbol{\tau}, \text{Re}_\star \frac{2R}{v_\star} \mathbf{v}_{\text{rel}} \right) \cdot \boldsymbol{\tau},$$

with normalized fiber tangent $\boldsymbol{\tau}$, $\|\boldsymbol{\tau}\| = 1$, and dimensionless drag function $\mathbf{F} : \mathbb{S}^2 \times \mathbb{R}^3 \rightarrow \mathbb{R}^3$ given in [12], where \mathbb{S}^2 denotes the three-dimensional sphere. The relative velocity between fiber and airflow reads $\mathbf{v}_{\text{rel}} = \mathbf{v}_\star - u\boldsymbol{\tau}$. Note that to distinguish the fiber quantities from the airflow quantities all airflow associated fields are labeled with the index \star . In particular, \mathbf{v}_\star denotes the velocity, ρ_\star the density, ν_\star the kinematic viscosity, λ_\star the thermal conductivity, and q_\star the specific heat capacity of the air. Moreover, $D_{d,\star}$ denotes the diffusivity of diluent in the air and $\rho_{d,\star}$ the diluent density in the air away from the fiber. All these quantities are space- and time-dependent fields assumed to be dimensionless and known—for example provided by an external computation. The corresponding reference values used for non-dimensionalization are denoted with the index $_0$ and given in Table 1. Furthermore, we employ the models for the heat and mass transfer

$$\begin{aligned} \alpha &= \frac{1}{\text{Nu}_\star} \frac{\lambda_\star}{2R} \mathcal{N} \left(\text{Re}_\star \frac{2R}{v_\star} \mathbf{v}_{\text{rel}} \cdot \boldsymbol{\tau}, \text{Re}_\star \frac{2R}{v_\star} \|\mathbf{v}_{\text{rel}}\|, \text{Pr}_\star \frac{q_\star \rho_\star \nu_\star}{\lambda_\star} \right), \\ \gamma &= \beta \varrho_\star, \quad c_{\text{ref}} = 1 - \frac{\rho_{d,\star}}{\varrho_\star}, \\ \beta &= \frac{1}{\text{Sh}_\star} \frac{D_{d,\star}}{2R} \mathcal{N} \left(\text{Re}_\star \frac{2R}{v_\star} \mathbf{v}_{\text{rel}} \cdot \boldsymbol{\tau}, \text{Re}_\star \frac{2R}{v_\star} \|\mathbf{v}_{\text{rel}}\|, \text{Sc}_\star \frac{\nu_\star}{D_{d,\star}} \right) \end{aligned}$$

with the associated dimensionless function $\mathcal{N} : \mathbb{R}^3 \rightarrow \mathbb{R}$ and the model for the diluent density in the air at the fiber surface ϱ_* given in [19]. The closing of System 2 requires further models for the diffusion coefficient D , thermal conductivity C , evaporation enthalpy δ , specific heat capacities q_p^0, q_d^0 , dynamic viscosity μ as well as material densities ρ_p^0, ρ_d^0 . For our industrial setup in Sect. 5 we employ detailed models taking the fiber materials and rheological effects into account.

4 Numerical framework

The fiber model for dry spinning of a single straight fiber (System 2) is a coupled system of one- and two-dimensional model equations. While the one-dimensional equations (2a) can be formulated as parametric boundary value problem of ordinary differential equations, the two-dimensional equations (2b) form a system of radial advection-diffusion equations with Robin-type boundary conditions. In [19] we presented a numerical framework for these two subproblems together with an iterative coupling procedure that made simulations of dry spinning processes feasible. However, when multiple hundred fibers are spun simultaneously and a two-way coupling with the surrounding airflow has to be taken into account, the simulations are still very time-consuming and can easily involve unfeasible computation times for industrial setups. When solving the coupled one-two-dimensional problem, it turns out that the computation of the two-dimensional profiles of polymer mass fraction and fiber temperature forms the bottleneck. In this section we, therefore, develop an algorithmic procedure to speed up the computation of these quantities. The key idea is that no radial profiles have to be computed in scenarios, where only surface and averaged values of the two-dimensional quantities are needed. The associated computation then simplifies to the solution of an integral equation and an ordinary differential equation. In the numerical treatment the solution of the integral equation reduces to the solution of a linear system of equations with lower triangular system matrix, such that it can be solved by forward substitution. When two-dimensional profiles are needed, e.g., for the dynamic viscosity (cf. Remark 3), we propose a new algorithm. In the following we give a general description of the coupled problem, present our new numerical strategies, describe the strategy for the iterative solving of the coupled problem, and give a survey for the further weak iterative coupling with an airflow simulation.

4.1 General problem formulation

To illustrate the structure of System 2, we embed it into the class of problems that consist of a one-dimensional boundary value problem of the form

$$\begin{aligned} &\text{Find } \mathbf{y} : [0, 1] \rightarrow \mathbb{R}^N \text{ with} \\ &\partial_s \mathbf{y}(s) = \mathbf{f}(\mathbf{y}(s), \boldsymbol{\psi}(\cdot, s), s), \quad s \in (0, 1), \\ &\mathbf{0} = \mathbf{g}(\mathbf{y}(0), \mathbf{y}(1), \boldsymbol{\psi}(\cdot, 0), \boldsymbol{\psi}(\cdot, 1)), \end{aligned}$$

coupled with a two-dimensional radial advection-diffusion equation of the form

$$\begin{aligned} &\text{Find } \boldsymbol{\psi} : [0, 1]^2 \rightarrow \mathbb{R}^M \text{ with} \\ &\partial_s \boldsymbol{\psi}(r, s) - \text{diag}(\boldsymbol{\lambda}(\mathbf{y}(s), \hat{\boldsymbol{\psi}}(\cdot, s), s)) \cdot \frac{1}{r} \partial_r (r \partial_r \boldsymbol{\psi}(r, s)) = \mathbf{0}, \quad (r, s) \in (0, 1)^2, \end{aligned}$$

$$\begin{aligned} \partial_s \psi(0, s) &= \mathbf{0}, \quad s \in (0, 1), \\ \partial_s \psi(1, s) - \text{diag}(\mathbf{c}(\mathbf{y}(s), \hat{\psi}(\cdot, s), s)) \cdot \psi(1, s) - \mathbf{d}(\mathbf{y}(s), \hat{\psi}(\cdot, s), s)) &= \mathbf{0}, \quad s \in (0, 1), \\ \psi(r, 0) &= \psi_{\text{in}}, \quad r \in [0, 1], \end{aligned}$$

with given right hand side functional $\mathbf{f} : \mathbb{R}^N \times \mathcal{C}^1((0, 1), \mathbb{R}^M) \times [0, 1] \rightarrow \mathbb{R}^N$, boundary functional $\mathbf{g} : \mathbb{R}^N \times \mathbb{R}^N \times \mathcal{C}^1((0, 1), \mathbb{R}^M) \times \mathcal{C}^1((0, 1), \mathbb{R}^M) \rightarrow \mathbb{R}^Q$, and the further functionals $\lambda, \mathbf{c}, \mathbf{d} : \mathbb{R}^N \times \mathcal{C}^1((0, 1), \mathbb{R}^M) \times [0, 1] \rightarrow \mathbb{R}^M$, the constant $\psi_{\text{in}} \in \mathbb{R}^M$ and $N, M, Q \in \mathbb{N}$. Moreover, we write $\text{diag}(\mathbf{k}) \in \mathbb{R}^{M \times M}$ for the diagonal matrix with entries $\mathbf{k} \in \mathbb{R}^M$. To illustrate the dependencies and to enable a decoupling of the problem for its numerical treatment, we introduce the help function $\hat{\psi} : [0, 1]^2 \rightarrow \mathbb{R}^M$. Note that for System 2 we have $\hat{\psi} = \psi$ as well as $\mathbf{g}(\mathbf{y}(0), \mathbf{y}(1), \psi(\cdot, 0), \psi(\cdot, 1)) = \mathbf{g}(\mathbf{y}(0), \mathbf{y}(1))$, and $N = M = Q = 2$.

To clarify the structure of the problem in view of its numerical treatment, we formally introduce (without discussing existence and uniqueness) the solution operators $B : \mathcal{C}^1((0, 1)^2, \mathbb{R}^M) \rightarrow \mathcal{C}^1((0, 1), \mathbb{R}^N)$ and $D : \mathcal{C}^1((0, 1), \mathbb{R}^N) \times \mathcal{C}^1((0, 1)^2, \mathbb{R}^M) \rightarrow \mathcal{C}^1((0, 1)^2, \mathbb{R}^M)$ associated to the one- and two-dimensional problems with $B[\psi] = \mathbf{y}$ and $D[\mathbf{y}, \hat{\psi}] = \psi$, respectively. Then, the coupled problem reads

$$\begin{aligned} \text{Find } \mathbf{y} : [0, 1] &\rightarrow \mathbb{R}^N \text{ and } \psi : [0, 1]^2 \rightarrow \mathbb{R}^M \text{ with} \\ \mathbf{y} - B[\psi] &= \mathbf{0}, \\ \psi - D[\mathbf{y}, \psi] &= \mathbf{0}. \end{aligned} \tag{3a}$$

The diffusion coefficient and boundary conditions in the radial advection-diffusion equation in (3a) depend on the variable ψ such that the associated problem is nonlinear. This nonlinearity is tackled by decoupling into the following two problems

$$\begin{aligned} \text{Find } \mathbf{y} : [0, 1] &\rightarrow \mathbb{R}^N \text{ with} \\ \mathbf{y} - B[\psi] &= \mathbf{0}, \end{aligned} \tag{3b}$$

for given function ψ and

$$\begin{aligned} \text{Find } \psi : [0, 1]^2 &\rightarrow \mathbb{R}^M \text{ with} \\ \psi - D[\mathbf{y}, \hat{\psi}] &= \mathbf{0} \end{aligned} \tag{3c}$$

for given functions $\mathbf{y}, \hat{\psi}$. In particular, we note that (3c) is a linear problem. Subsequently, we explain the respective numerical algorithms for the decoupled problems (3b), (3c) and discuss a coupling strategy to obtain a solution of the coupled problem (3a).

In view of the coupling we need the associated radial advection-diffusion equations averaged over the fiber cross-sections, which we already introduce here

$$\begin{aligned} \text{Find } \bar{\psi} : [0, 1] &\rightarrow \mathbb{R}^M \text{ with} \\ \partial_s \bar{\psi}(s) &= 2 \text{diag}(\lambda(\mathbf{y}(s), \hat{\psi}(\cdot, s), s)) \\ &\quad \cdot (\text{diag}(\mathbf{c}(\mathbf{y}(s), \hat{\psi}(\cdot, s), s)) \cdot \psi(1, s) + \mathbf{d}(\mathbf{y}(s), \hat{\psi}(\cdot, s), s)), \quad s \in (0, 1), \\ \bar{\psi}(0) &= \psi_{\text{in}}. \end{aligned}$$

We make use of the corresponding formal solution operator $\bar{D} : \mathcal{C}^1((0, 1), \mathbb{R}^N) \times \mathcal{C}^1((0, 1)^2, \mathbb{R}^M) \times \mathcal{C}^1((0, 1), \mathbb{R}^M) \rightarrow \mathcal{C}^1((0, 1), \mathbb{R}^M)$, such that the averaged problem can be written as

$$\begin{aligned} &\text{Find } \bar{\psi} : [0, 1] \rightarrow \mathbb{R}^M \text{ with} \\ &\bar{\psi} - \bar{D}[\mathbf{y}, \hat{\psi}, \psi|_{r=1}] = \mathbf{0} \end{aligned} \tag{4}$$

for given functions $\mathbf{y}, \hat{\psi}, \psi|_{r=1}$.

4.2 Boundary value problem algorithm

We consider the one-dimensional boundary value problem (3b) and assume the function ψ to be given. This means $\mathbf{f}(\mathbf{y}(s), \psi(\cdot, s), s) = \mathbf{f}(\mathbf{y}(s), s)$ and $\mathbf{g}(\mathbf{y}(0), \mathbf{y}(1), \psi(\cdot, 0), \psi(\cdot, 1)) = \mathbf{g}(\mathbf{y}(0), \mathbf{y}(1))$, and (3b) can be summarized as

$$\partial_s \mathbf{y}(s) = \mathbf{f}(\mathbf{y}(s), s), \quad \mathbf{g}(\mathbf{y}(0), \mathbf{y}(1)) = \mathbf{0}, \tag{5}$$

on the domain $[0, 1]$. Since the function \mathbf{f} depends on multiple parameters, the numerical challenge lies in solving the problem for arbitrary parameter settings, which requires suitable initial guesses of the respective solutions. As in our previous works [1, 19, 20] we tackle this problem by a continuation-collocation method. This means we use a three-stage Lobatto IIIa formula as collocation scheme [10], which is a Runge–Kutta scheme of fourth order

$$\begin{aligned} &\mathbf{y}_{i+1} - \mathbf{y}_i - \frac{h_{i+1}}{6} (\mathbf{f}(\mathbf{y}_i, s_i) + 4\mathbf{f}(\mathbf{y}_{i+1/2}, s_{i+1/2}) + \mathbf{f}(\mathbf{y}_{i+1}, s_{i+1})) = \mathbf{0}, \quad \mathbf{g}(\mathbf{y}_0, \mathbf{y}_N) = \mathbf{0}, \\ &\text{with } \mathbf{y}_{i+1/2} = \frac{1}{2}(\mathbf{y}_{i+1} + \mathbf{y}_i) - \frac{h_{i+1}}{8} (\mathbf{f}(\mathbf{y}_{i+1}, s_{i+1}) - \mathbf{f}(\mathbf{y}_i, s_i)), \end{aligned}$$

with collocation points $\mathbf{0} = s_0 < s_1 < \dots < s_{N_s} = 1$, intermediate points $s_{i+1/2} = (s_i + s_{i+1})/2$, mesh size $h_i = s_i - s_{i-1}$ and the abbreviation $\mathbf{y}_i = \mathbf{y}(s_i)$, $i = 0, \dots, N_s$. The resulting nonlinear system of $N_s + 1$ equations for $(\mathbf{y}_i)_{i=0, \dots, N_s}$ is solved using a Newton method with numerically approximated Jacobian matrix. Since the convergence of the Newton method crucially depends on the initial guess, we adapt the initial guess iteratively by means of a continuation method, solving a sequence of slightly varying boundary value problems. In the continuation method we embed the boundary value problem (5) into a family of problems by introducing a continuation parameter tuple $\mathbf{p} \in [0, 1]^n$, $n \in \mathbb{N}$,

$$\begin{aligned} &\frac{d}{ds} \mathbf{y} = \hat{\mathbf{f}}(\mathbf{y}; \mathbf{p}), \quad \hat{\mathbf{g}}(\mathbf{y}(0), \mathbf{y}(1); \mathbf{p}) = \mathbf{0}, \quad \mathbf{p} \in [0, 1]^n, \\ &\hat{\mathbf{f}}(\cdot; \underline{\mathbf{1}}) = \mathbf{f}, \quad \hat{\mathbf{g}}(\cdot, \cdot; \underline{\mathbf{1}}) = \mathbf{g}, \quad \mathbf{f}(\cdot; \mathbf{0}) = \mathbf{f}_0, \quad \hat{\mathbf{g}}(\cdot, \cdot; \mathbf{0}) = \mathbf{g}_0. \end{aligned}$$

Here, $\underline{\mathbf{1}} \in \mathbb{R}^n$ denotes the n -dimensional tuple of ones. The functions $\mathbf{f}_0, \mathbf{g}_0$ are chosen in such a way that for $\mathbf{p} = \mathbf{0}$ an analytical solution is known. Given this starting solution, we seek for a sequence of parameter tuples $\mathbf{0} = \mathbf{p}_0, \mathbf{p}_1, \dots, \mathbf{p}_m = \underline{\mathbf{1}}$ such that the solution to the respective predecessor boundary value problem provides a good initial guess for the successor. The solution associated to $\mathbf{p} = \underline{\mathbf{1}}$ finally belongs to the original system. With the help of the continuation parameters certain terms in the ordinary differential equation can be first excluded, then included. Also the boundary conditions can be varied. The

core of a robust continuation procedure are the choice of a continuation path and the step size control to navigate through a high-dimensional parameter space. They decide about failure or success because there are not always existing solutions and several ways might be possible. For the choice of the continuation path we refer to [19] and the step size control follows the strategy given in [2].

4.3 Radial advection-diffusion equation algorithm

We consider (3c) with given functions $\mathbf{y}, \hat{\psi}$. This means $\lambda(\mathbf{y}(s), \hat{\psi}(\cdot, s), s) = \lambda(s)$, such that the problem becomes linear. Furthermore, we transform the unknown ψ by the following rule

$$\chi_i(r, \Lambda_i(s)) = \psi_i(r, s), \quad \text{with } \Lambda_i(s) = \int_0^s \lambda_i(s') \, ds', \quad i = 1, \dots, M,$$

where y_i denotes the i -th component of any vector field \mathbf{y} . For any component $\chi_i, i \in \{1, \dots, M\}$, we end up with a radial advection-diffusion equation of the form

$$\begin{aligned} \partial_x \phi - \frac{1}{r} \partial_r (r \partial_r \phi) &= 0, \\ \phi|_{x=0} &= \phi_{\text{in}}, \quad \partial_r \phi|_{r=0} = 0, \quad \partial_r \phi|_{r=1} = a\phi|_{r=1} + b, \end{aligned}$$

with $\phi : [0, 1]^2 \rightarrow \mathbb{R}, (r, x) \mapsto \phi(r, x)$, as well as functions $a, b : [0, 1] \rightarrow \mathbb{R}$ and constant $\phi_{\text{in}} \in \mathbb{R}$. If the function a is constant, the solution can be given analytically in terms of an explicit expression. For non-constant a we treat the Robin boundary condition as Neumann boundary condition with right hand side depending on ϕ and find an implicit solution expression with Green's function g in [3, 7, 16]. The solution expression reads

$$\begin{aligned} \phi(r, x) &= \phi_{\text{in}} + 2\pi \int_0^x g(r, x - x') k(x', \phi(1, x')) \, dx', \\ \text{with } g(r, x) &= \frac{1}{\pi} \left(1 + \sum_{m=1}^{\infty} \frac{J_0(\beta_m r)}{J_0(\beta_m)} \exp(-\beta_m^2 x) \right), \quad k(x, y) = a(x)y + b(x), \end{aligned} \tag{6}$$

where J_i denote the i -th Bessel functions of first kind and $\beta_m > 0, m \in \mathbb{N}$, are the (non-trivial) ascending zeros of the first Bessel function of first kind, i.e., $J_1(\beta_m) = 0$. These values are tabulated in literature, see e.g. [7]. For $\phi|_{r=1}$ the solution expression yields a Volterra integral equation of second kind

$$\begin{aligned} \phi(1, x) &= \phi_{\text{in}} + 2\pi \int_0^x g(1, x - x') k(x', \phi(1, x')) \, dx', \\ \text{with } g(1, x) &= \frac{1}{\pi} \left(1 + \sum_{m=1}^{\infty} \exp(-\beta_m^2 x) \right). \end{aligned} \tag{7}$$

The integral kernel g is singular for $x = 0$. Therefore, numerical integration in the sense of quadrature formulas cannot be applied directly to the integral in (7), because they involve the evaluation of the integrand function at or close to the singularity. Hence, we use the product integration method that we introduced in [18, 19]. This means we substitute the function $k(\cdot, \phi(1, \cdot))$ piecewise by Lagrange interpolation polynomials and employ iterated

integration by parts to isolate the singularity of the kernel function g . Here, we choose constant polynomials corresponding to the implicit Euler method yielding an A- and L-stable method. For the discussion of stability properties as well as an extension to a higher order method with quadratic polynomials and nodes corresponding to the Lobatto IIIa collocation scheme we refer to [19].

Let $0 = x_0 < x_1 < \dots < x_{N_x} = 1$ be the mesh points in x -direction. Substituting the integrand function $k(\cdot, \phi(1, \cdot))$ piecewise by constants in the sense of the implicit Euler scheme and subsequent integration yields

$$\begin{aligned} \phi_i(1) &= \phi_0(1) + 2\pi \sum_{j=1}^i \int_{x_{j-1}}^{x_j} g(1, x_i - x') k(x_j, \phi_j(1)) dx' \\ &= \phi_0(1) + 2\pi \sum_{j=1}^i (-g_{ij}^{(-1)}(1) + g_{ij-1}^{(-1)}(1)) k(x_j, \phi_j(1)), \quad i = 1, \dots, N_x, \end{aligned}$$

with $\phi_i(r) = \phi(r, x_i)$, $\phi_0(r) = \phi_{in}$, and the primitive

$$\begin{aligned} g_{ij}^{(-1)}(r) &= g^{(-1)}(r, x_i - x_j), \\ g^{(-1)}(r, x) &= \int_0^x g(r, x') dx' = \frac{1}{\pi} \left(x + \sum_{m=1}^{\infty} \frac{J_0(\beta_m r)}{\beta_m^2 J_0(\beta_m)} (1 - \exp(-\beta_m^2 x)) \right), \end{aligned}$$

which we evaluated analytically. This results in the linear system of equations

$$(\mathbf{I} - 2\pi \mathbf{G}(1) \cdot \text{diag}(\mathbf{a})) \cdot \boldsymbol{\phi}(1) = \boldsymbol{\phi}_{in} + 2\pi \mathbf{G}(1) \cdot \mathbf{b}$$

for the unknown vector $\boldsymbol{\phi}(1) = (\phi_1(1), \dots, \phi_{N_x}(1)) \in \mathbb{R}^{N_x}$. Here, $\boldsymbol{\phi}_{in} = \phi_{in} \mathbf{1} \in \mathbb{R}^{N_x}$ with $\mathbf{1} \in \mathbb{R}^{N_x}$ the N_x -dimensional tuple of ones and $\mathbf{I} \in \mathbb{R}^{N_x \times N_x}$ denotes the identity matrix. The matrix $\mathbf{G}(r) = (G_{ij}(r))_{i,j=1, \dots, N_x} \in \mathbb{R}^{N_x \times N_x}$ is defined as

$$G_{ij}(r) = \begin{cases} -g_{ij}^{(-1)}(r) + g_{ij-1}^{(-1)}(r), & \text{if } 1 \leq j \leq i, \\ 0, & \text{else.} \end{cases}$$

Furthermore, we use the vectors $\mathbf{a} = (a_1, \dots, a_{N_x}) \in \mathbb{R}^{N_x}$, $\mathbf{b} = (b_1, \dots, b_{N_x}) \in \mathbb{R}^{N_x}$ using the abbreviations $a_i = a(x_i)$, $b_i = b(x_i)$. The system matrix $(\mathbf{I} - 2\pi \mathbf{G}(1) \cdot \text{diag}(\mathbf{a}))$ is lower triangular, such that the linear system of equations can be solved by forward substitution.

After solution of the integral equation for the boundary values $\boldsymbol{\phi}(1)$ the profile $\boldsymbol{\phi}(r) = (\phi_1(r), \dots, \phi_{N_x}(r)) \in \mathbb{R}^{N_x}$, $0 \leq r \leq 1$, can be calculated at the mesh points x_i using the same approximation strategy for the singular integral

$$\boldsymbol{\phi}(r) = \boldsymbol{\phi}_{in} + 2\pi \mathbf{G}(r) \cdot \mathbf{d}\boldsymbol{\phi}(1) \quad \text{with } \mathbf{d}\boldsymbol{\phi}(1) = \text{diag}(\mathbf{a}) \cdot \boldsymbol{\phi}(1) + \mathbf{b}.$$

For the calculation of the matrix $\mathbf{G}(r)$, we define further lower triangular matrices $\mathbf{H}(\beta_m) = (H_{ij}(\beta_m))_{i,j=1, \dots, N_x} \in \mathbb{R}^{N_x \times N_x}$ and $\mathbf{\Delta} = (\Delta_{ij})_{i,j=1, \dots, N_x} \in \mathbb{R}^{N_x \times N_x}$ as

$$H_{ij}(\beta_m) = \begin{cases} \exp(-\beta_m^2(x_i - x_j)) - \exp(-\beta_m^2(x_i - x_{j-1})), & \text{if } 1 \leq j \leq i, \\ 0, & \text{else,} \end{cases}$$

and

$$\Delta_{ij} = \begin{cases} x_j - x_{j-1}, & \text{if } 1 \leq j \leq i, \\ 0, & \text{else.} \end{cases}$$

Thus, we can re-write the entries of $\mathbf{G}(r)$

$$G_{ij}(r) = \frac{1}{\pi} \left(\Delta_{ij} + \sum_{m=1}^{\infty} H_{ij}(\beta_m) B(\beta_m, r) \right), \quad B(\beta_m, r) = \frac{J_0(\beta_m r)}{\beta_m^2 J_0(\beta_m)},$$

and the profiles are given as

$$\phi(r) = \phi_{in} + 2\Delta \cdot \mathbf{d}\phi(1) + 2 \sum_{m=1}^{\infty} (\mathbf{H}(\beta_m) \cdot \mathbf{d}\phi(1)) B(\beta_m, r). \tag{8}$$

Due to the separation of the r -dependency and its exclusive occurrence in the factor B , this representation allows an efficient implementation of the calculation of the profiles with complexity in $\mathcal{O}(\max\{N_x^2 N_\beta, N_r\})$ with N_β the number of zeros β_m of J_1 taken into account for the calculation. This is a great improvement compared to the implementation given in [19] that has the complexity $\mathcal{O}(N_x^2 N_\beta N_r)$.

In view of System 2 the cross-sectionally averaged quantity $\bar{\phi}$ is needed. This quantity can be obtained with the help of two different approaches

- Method 1: Averaging of the profiles,
- Method 2: Solution of the integrated advection-diffusion equation.

In *Method 1* the calculation follows directly from the profiles

$$\bar{\phi}(x) = 2 \int_0^1 \phi(r, x) r \, dr. \tag{9a}$$

Introducing a mesh in r -direction, $0 = r_0 < \dots < r_{N_r} = 1$, $N_r \in \mathbb{N}$, and utilizing the trapezoidal rule we get

$$\bar{\phi}_i = \sum_{j=1}^{N_r} (\phi(r_{j-1}, x_i) r_{j-1} + \phi(r_j, x_i) r_j) (r_j - r_{j-1}), \quad i = 0, \dots, N_x.$$

The complexity of Method 1 is $\mathcal{O}(N_x N_r)$.

In *Method 2* the averaged quantity $\bar{\phi}$ is calculated with the help of the integrated advection-diffusion equation (4) that reads component-wisely after transformation onto the x -grid

$$\partial_x \bar{\phi} = 2(a(x)\phi(1, x) + b(x)), \quad \bar{\phi}(r, 0) = \phi_{in}. \tag{9b}$$

This differential equation can be solved by integration with respect to x omitting any discretization error in radial direction. Employing right Riemann summation, which corresponds to the product integration method based on the implicit Euler scheme, we get the recursion formula

$$\bar{\phi}_0 = \phi_{in}, \quad \bar{\phi}_i = \bar{\phi}_{i-1} + 2 \, \mathbf{d}\phi_i(1)(x_i - x_{i-1}), \quad i = 1, \dots, N_x.$$

In difference to Method 1, Method 2 omits any radial resolution and has the lower complexity of $\mathcal{O}(N_x)$. Moreover, in situations where only boundary $\phi|_{r=1}$ and averaged values $\bar{\phi}$ are needed the calculation of two-dimensional profiles ϕ can be omitted completely when Method 2 is used. Thus, Method 2 is obviously preferable to Method 1 due to efficiency reasons.

4.4 Coupling procedure

For the solution of (3a) we proposed an iterative coupling of the solution algorithm for the one-dimensional boundary value problem with the solution algorithm for the radial advection-diffusion equation in [19]. Here, we formulate this coupling procedure with respect to the general problem formulation given in Sect. 4.1.

In view of the radial advection-diffusion equation a solution of the integrated problem (4) based on averaged quantities serves as initial guess in our coupling procedure. Since we employ the profiles of polymer mass fraction c and temperature T to approximate the averaged dynamic viscosity $\langle \mu(c, T) \rangle_{R^2} / (\pi R^2)$ (cf. Remark 3) we have to build up the two-dimensional profiles of these quantities. In total the coupling of the one- and two-dimensional model equations is done as described in Algorithm 1.

In the coupling procedure (Algorithm 1) cross-sectionally averaged quantities are needed for the solution of the one-dimensional boundary value problem in Line 5, i.e., cross-sectionally averaged quantities propagate into the operator B. These averaged quantities have to be calculated after the computation of the two-dimensional quantities ψ^{i+1} in Line 4. This can be done by either of the Methods 1 or 2. In view of its implementation Method 2, which involves the solution of the integrated equation (4), needs further considerations. We introduce two submethods for the computation of the averaged quantity $\bar{\psi}^{i+1}$:

- Method 2a: Solve $\bar{\psi}^{i+1} - \bar{D}[\mathbf{y}^i, \psi^i, (\psi|_{r=1})^i] = \mathbf{0}$,
- Method 2b: Solve $\bar{\psi}^{i+1} - \bar{D}[\mathbf{y}^{i+1}, \psi^{i+1}, (\psi|_{r=1})^{i+1}] = \mathbf{0}$.

This means, *Method 2a* utilizes the profile information from the preceding iteration step, whereas *Method 2b* uses the updated information from the actual iteration step. At first glance, Method 2b looks more straightforward but it has a major drawback: The nonlinearity of the coupled problem (3a) comes from the nonlinearity of the one-dimensional and two-dimensional equations themselves as well as the nonlinear coupling of these equations. Whereas the nonlinearity of the one-dimensional equations is treated by the continuation method, the remaining nonlinearities in common are tackled iteratively by Algorithm 1. This means, ψ^{i+1} as calculated in Line 4 is only a solution of $\psi^{i+1} - D[\mathbf{y}^i, \psi^{i+1}]$ when Algorithm 1 is converged. Therefore, when solving the integrated equation (4), $\bar{\psi}^{i+1}$

Algorithm 1 Coupling procedure for fiber solution

- 1: $(\mathbf{y}^0, \bar{\psi}^0) \leftarrow \text{Solve } (\mathbf{y}^0, \bar{\psi}) - (B[\bar{\psi}], \bar{D}[\mathbf{y}^0, \bar{\psi}, \bar{\psi}]) = \mathbf{0}$
 - 2: $i \leftarrow 0$
 - 3: **repeat**
 - 4: $\psi^{i+1} \leftarrow \text{Solve } \psi^{i+1} - D[\mathbf{y}^i, \psi^i] = \mathbf{0}$
 - 5: $\mathbf{y}^{i+1} \leftarrow \text{Solve } \mathbf{y}^{i+1} - B[\psi^{i+1}] = \mathbf{0}$
 - 6: $i \leftarrow i + 1$
 - 7: **until** $\|(\mathbf{y}^i, \psi^i) - (\mathbf{y}^{i+1}, \psi^{i+1})\| < tol$
-

coincides only with the averaged value of ψ^{i+1} , when Method 2a is employed. Method 2b, however, yields an inconsistent averaged quantity $\bar{\psi}^{i+1}$. The equivalence of the cross-sectionally averaged quantities as a result from Method 2a and Method 2b is only assured when the coupling procedure (Algorithm 1) is converged. We exemplify this issue with the help of our numerical results given in Sect. 5.

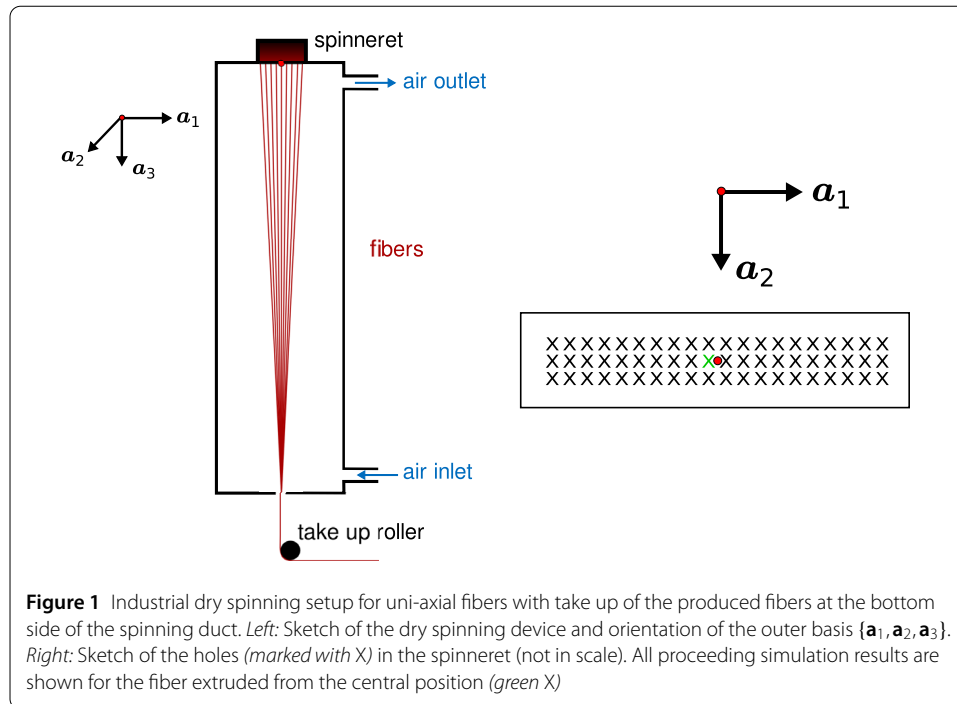
Remark 4 (Two-way fiber-air interaction) Since the nature of the airflow in the spinning duct has a deep impact onto the behavior of the fibers and also the fibers itself affect the properties of the airflow, a two-way coupling between the fibers and the airflow has to be taken into account. This coupling is realized by homogenized exchange models. The exchange models are constructed in such a way, that the principle of action equaling reaction is fulfilled, cf. [5, 6]. The two-way fiber-air-interaction is realized by a weak coupling algorithm which iterates between fiber computations and airflow simulations. This procedure allows the combination of self-implemented code for the fiber dynamics as well as a commercial software for the air dynamics and was successfully used in studies on glass wool manufacturing [2]. In total, our complete procedure consists of nested iterations: An inner iteration for the coupling of one- and two-dimensional fiber equations (Algorithm 1) and an outer iteration realizing the mutual fiber-airflow interaction. For further details we refer to [19].

5 Industrial application

In this section, we consider the industrial example of [19] and investigate the performance of the new numerical methods. In particular, we highlight the efficiency of the calculation of two-dimensional profiles (c, T) using the representation (8) and compare Method 1, Method 2a and Method 2b for the computation of cross-sectionally averaged quantities (\bar{c}, \bar{T}) . Note that for the sake of clarity we use dimensionful quantities to describe the following setup and results.

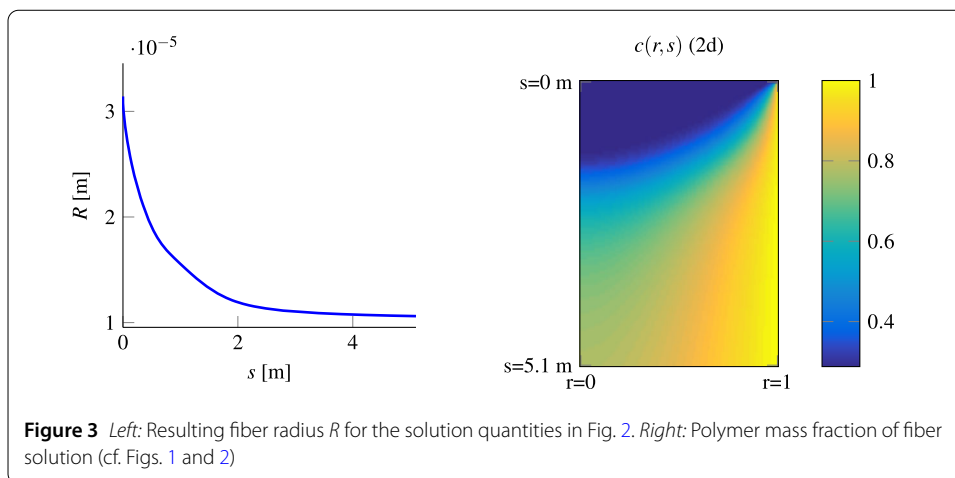
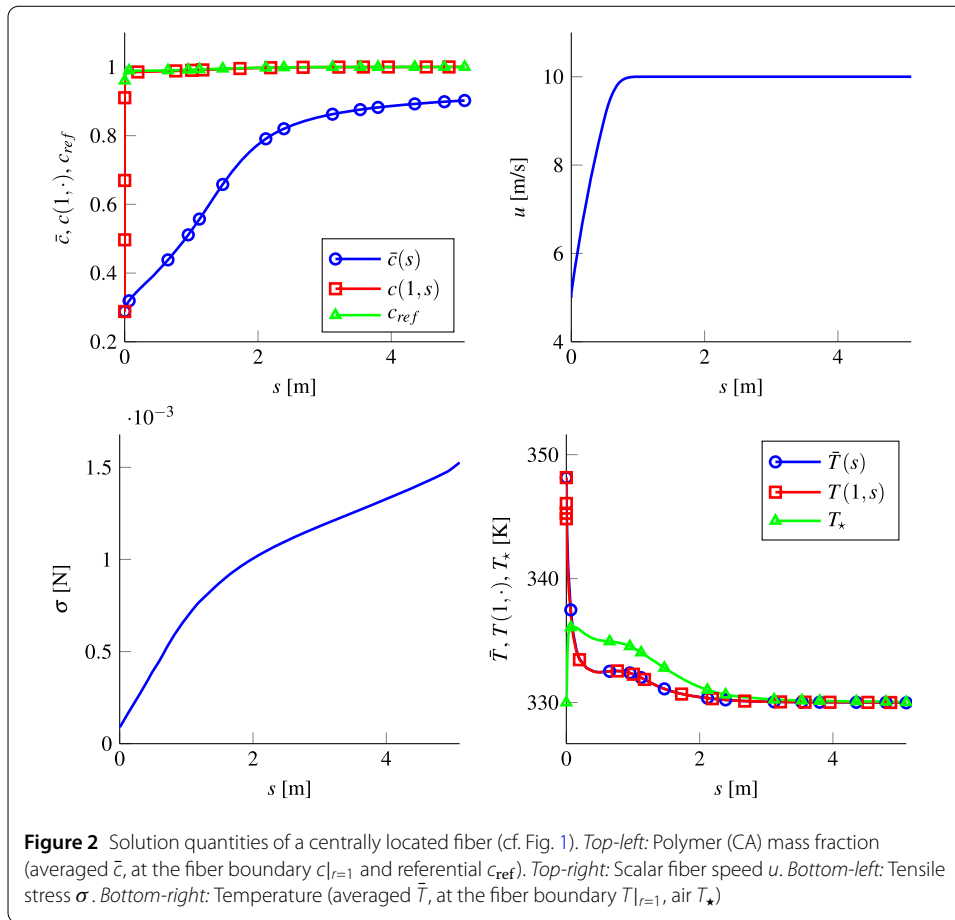
Remark 5 Algorithm 1 is implemented in MATLAB^a version R2016b, where the BVP solver `bvp4c.m` is used with the default values. For the computation of the two-dimensional profiles we choose $N_r = 201$ equidistant points in r -direction and $N_\beta = 318$, i.e., we use all non-trivial zeros of J_1 smaller than 10^3 . As stopping criterion for the iteration in Algorithm 1 we use $tol = 10^{-6}$. For the simulation of the airflow we employ ANSYS Fluent^b with a solver accuracy of $\mathcal{O}(10^{-6})$. The break-up criterion of the fiber-air coupling algorithm satisfies an error tolerance $tol = 10^{-5}$. For the considered industrial setup the fiber-air coupling algorithm converges after 30 iteration steps.

In the setup 60 fibers are spun in a spinning duct and drawn down by a take up roller at the duct bottom. The length L and tangent vector τ of a fiber are given through its inflow position in the spinneret and the position of the take up at the bottom. We consider the outer basis $\{\mathbf{a}_1, \mathbf{a}_2, \mathbf{a}_3\} \subset \mathbb{R}^3$ as given in Fig. 1. The holes in the spinneret are ordered in three parallel rows with 20 holes each. In particular, we consider the fibers of the middle row to be spun in the x_1 - x_3 -plane corresponding to $x_2 = 0$. The airflow forms a counter-current to the fiber flow and we assume dry air at the inlet (pipe radius $R_{*,in} = 9.8 \cdot 10^{-2}$ m) with an absolute air inflow velocity (in negative \mathbf{a}_1 -direction) at the bottom pipe of $\|\mathbf{v}_*\| = 0.22$ m/s and air inflow temperature $T_* = 330$ K. A cellulose acetate (CA)-acetone mixture is dry

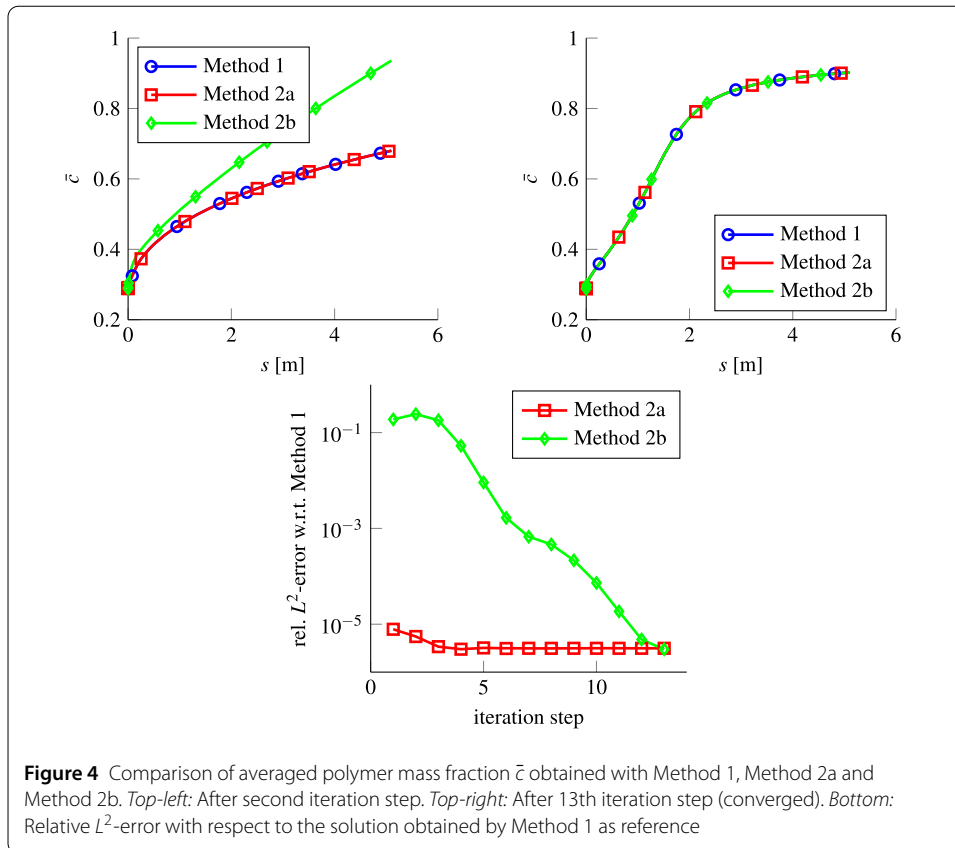


spun. For the closing of our dry spinning model (System 2) we employ rheological models for the quantities C , D , h_d^0 , δ , μ that are given in [19]. All further process parameters, the specific reference values as well as the dimensionless numbers are listed in the Appendix.

Cellulose acetate/acetone dry spinning was previously also investigated in [9, 17]. The results obtained by our model-simulation framework in [19] stand in accordance to the data in [17]. Exchanging the algorithmic by the new numerical methods (developed in Sect. 4) has no effect on the approximation quality, but only on the computational effort of the simulation. However, before we discuss the performance of the new methods, we present the simulation outcome to illustrate the typical fiber behavior for an industrial dry spinning setup. The solutions of the 60 fibers do not show visible differences, such that we illustrate—as an example—the solution behavior for the fiber that is centrally located in the spinning duct (cf. Fig. 1) in Fig. 2. The cross-sectionally averaged CA mass fraction increases from $c_0 = 0.29$ at the inlet to $\bar{c} = 0.90$ at the outlet, indicating the evaporation of the acetone during the spinning process. The fiber speed u reaches the take up speed $u_{\text{out}} = 10$ m/s approximately 1 m away from the nozzle. The tensile stress σ increases correspondingly to the changes of u and the integrated viscosity $\langle \mu \rangle_{R^2}$. Directly at the nozzle the fiber loses heat due to acetone evaporation and away from the nozzle the fiber temperature approaches the airflow temperature. The fiber thinning is caused by the fiber take up as well as the evaporation of diluent. The final fiber radius is $R = 1.06 \cdot 10^{-5}$ m (cf. Fig. 3). The effect of solvent diffusion in the fiber interior can clearly be seen at the profile for the polymer mass fraction in Fig. 3 showing an inhomogeneous CA-acetone distribution in radial direction. Since there are no visible radial effects in the temperature due to the fact that the inverse of the temperature associated Peclet number $1/\text{Pe}_T$ is three magnitudes larger compared to the mass associated one $1/\text{Pe}_c$ (cf. Table 4) we omit to show a radial temperature profile.



Investigating the performance of the new numerical methods, first, we highlight the efficiency of the calculation of profiles using the representation (8). Whereas in [19] the total simulation time with a straightforward implementation for the profile solution (regardless of (8)) was 7.95 h, the simulation only needs 5.20 h utilizing the efficient profile calculation (cf. (8)) here, which means a reduction of 34.6% in total. Exemplarily considering $N_r = 201$ and $N_x = 501$ points in r - and x -direction for the profiles as well as $N_\beta = 318$, the calcu-



lation time for one single profile reduces from 97.89 s to 0.94 s. Thus, in view of spinning setups where multiple hundred fibers are spun simultaneously this efficiency in the profile computation is absolutely essential.

Second, we compare the three different procedures (Method 1, Method 2a, and Method 2b) for the computation of the cross-sectionally averaged polymer mass fraction \bar{c} and consider Method 1 (averaging of two-dimensional profiles), which has been used in [19], as reference. We exemplarily consider the last step in the air-fiber coupling (30th iteration) where Algorithm 1 converges after 13 iteration steps. Figure 4 shows the results after the 2nd and the 13th iteration step. We clearly see that Method 2b initially produces an inconsistent solution due to the use of inconsistent profile information, see Sect. 4.4. The calculated averaged polymer mass fraction \bar{c} exceeds the average of the associated profile (solution obtained by Method 1) greatly. This behavior could lead to a completely unphysical solution behavior in the next iteration steps and even to a failure of the iterative coupling procedure (divergence of Algorithm 1). On the other hand, Method 2a yields a consistent solution. As soon as Algorithm 1 is converged, the solutions obtained with Method 1, Method 2a and Method 2b coincide. This fact can be seen in Fig. 4 indicating the relative L^2 -error between these three solutions with Method 1 as reference. Consequently, Method 2a should be used for the calculation of \bar{c} , \bar{T} . In view of computational time the difference between Method 1 and Method 2a is marginal. Whereas Method 1 takes $1.30 \cdot 10^{-3}$ s, Method 2a needs $3.42 \cdot 10^{-4}$ s for $N_x = 501$ points. However, the clear advantage of Method 2a comes into play when no two-dimensional profiles need to be calculated.

6 Conclusion

For the modeling of viscous fibers in dry spinning processes one-dimensional equations for tangential fiber velocity and stress coupled with two-dimensional radial advection-diffusion equations for polymer mass fraction and temperature are used. In this paper we introduced new algorithmic concepts for the fast computation of the two-dimensional information. The efficient calculation of surface values and averaged quantities as well as the speed up of the coupling procedure for one- and two-dimensional equations yields feasible computation times for simulations where multiple hundred fibers are spun simultaneously and mutual air-fiber interaction effects are incorporated. Consequently, our proposed model-simulation framework provides the possibility for optimizing industrial dry spinning devices. Depending on the mixture to be spun and the device the rheological models as well as the material and process parameters must be certainly adapted.

Appendix: Data to industrial process

In this paper (cf. Sect. 5) we consider the same dry spinning setup that was studied in [19] and demonstrate the performance of the new numerical methods (cf. Sect. 4). We assume that a polymer solvent mixture consisting of cellulose acetate (CA)-acetone is dry spun.

Table 2 Physical parameters of the industrial dry spinning setups taken from [9, 17] and setup-specific reference values

Physical parameters				Setup-specific reference values	
Description	Symbol	Value	Unit	Description	Formula
CA density	ρ_p^0	1300	kg/m ³	Mass line density	$Q_{M,0} = \rho(c_{in})R_{in}^2\pi$
Acetone density	ρ_d^0	767	kg/m ³	Curve	$r_0 = H$
CA spec. heat cap.	q_p^0	1600	J/(kg K)	Diameter	$d_0 = 2R_{in}$
Acetone spec. heat cap.	q_d^0	2160	J/(kg K)	Velocity	$v_0 = u_{in}$
Molec. weight acetone	M_d	$5.81 \cdot 10^{-2}$	kg/mol	Viscosity	$\mu_0 = \mu(c_{in}, T_{in})$
Molec. weight air	M_\star	$2.90 \cdot 10^{-3}$	kg/mol	Spec. heat cap.	$q_0 = q(c_{in})$
Molar volume acetone	V_d	$6.60 \cdot 10^{-5}$	m ³ /mol	Thermal cond.	$C_0 = C_{const}$
Molar volume air	V_\star	$2.01 \cdot 10^{-5}$	m ³ /mol	Diffusivity	$D_0 = D(c_{in}, T_{in})$
				Take up speed	$u_{out,0} = u_{out}$
				Further scales	$b_0 = b_{in}, b \in \{T, \alpha, \gamma, \rho_\star, \lambda_\star, \nu_\star, q_\star, \rho_\star, D_{d,\star}\}$

Table 3 Process parameters of the industrial dry spinning setup (cf. Fig. 1) assuming the airflow without fibers (first step in the fiber-airflow coupling)

Process parameters				
Description	Symbol	Value	Unit	
Device height	H	5.1	m	
Nozzle radius	R_{in}	$3.14 \cdot 10^{-5}$	m	
Speed at nozzle	u_{in}	5	m/s	
Take up speed at bottom	u_{out}	10	m/s	
Polym. mass fract. at nozzle	c_{in}	0.29	–	
Temperature at nozzle	T_{in}	348.15	K	
Total number of fibers	M	60	–	
Heat transfer at nozzle	α_{in}	$5.11 \cdot 10^2$	W/(m ² K)	
Mass transfer at nozzle	γ_{in}	1.64	kg/(m ² s)	
Air pressure at nozzle	$p_{\star,in}$	$1.01 \cdot 10^5$	Pa	
Air thermal cond. at nozzle	$\lambda_{\star,in}$	$2.42 \cdot 10^{-2}$	W/(m K)	
Air kin. viscosity at nozzle	$\nu_{\star,in}$	$1.46 \cdot 10^{-5}$	m ² /s	
Air spec. heat cap. at nozzle	$q_{\star,in}$	$1.01 \cdot 10^3$	J/(kg K)	
Air density at nozzle	$\rho_{\star,in}$	1.23	kg/m ³	
Diluent diffusion in air at nozzle	$D_{d,\star,in}$	$1.27 \cdot 10^{-5}$	m ² /s	

Table 4 Dimensionless numbers for one representative fiber (cf. Fig. 1) in the industrial dry spinning setup assuming the airflow without fibers (first step in the fiber-airflow coupling). Note that some dimensionless numbers might vary during the simulation due to the fiber-airflow interaction (cf. Table 1)

<i>Dimensionless numbers</i>		
Description	Symbol	Value
Slenderness	ε	$1.23 \cdot 10^{-5}$
Reynolds	Re	$1.79 \cdot 10^3$
Froude	Fr	$7.07 \cdot 10^{-1}$
Drawing	Dr	2.00
Mass Peclet	Pe_c	$4.16 \cdot 10^6$
Temperature Peclet	Pe_T	$2.73 \cdot 10^3$
Mass Stanton	St_c	$3.76 \cdot 10^{-4}$
Temperature Stanton	St_T	$5.88 \cdot 10^{-5}$
Air drag associated	A_*	$1.14 \cdot 10^2$
Air-fiber Reynolds	Re_*	$2.15 \cdot 10^1$
Nusselt	Nu_*	1.33
Prandtl	Pr_*	$7.44 \cdot 10^{-1}$
Sherwood	Sh_*	6.59
Schmidt	Sc_*	1.15

A similar setup has been investigated in [9, 17], from where we take the physical material parameters for the polymer CA and the diluent acetone, see Table 2. The setup-specific reference values used for the non-dimensional form of the model equations (cf. System 2) are also given in Table 2. All further process parameters can be found in Table 3. Utilizing the setup-specific reference values (cf. Table 2) the resulting dimensionless numbers are given in Table 4.

Acknowledgements

The authors acknowledge the support by German Federal Ministry of Education and Research (BMBF, Project VISP 03VP06651).

Funding

Not applicable.

Abbreviations

Not applicable.

Availability of data and materials

The datasets used and/or analyzed during the current study are included in this article and available from the authors on reasonable request.

Competing interests

The authors declare that they have no competing interests.

Authors' contributions

The success of this work is due to the strong and fruitful collaboration of all authors. Special merits go to MW for implementing the numerical schemes and performing the simulations. All authors read and approved the final manuscript.

Authors' information

The authors were invited to present their research on developments in mathematics for industrial dry spinning processes by European Consortium for Mathematics in Industry (ECMI)—as selected contribution of the ECMI 2018 Conference, Budapest, June 18–22.

Author details

¹Fraunhofer ITWM, Kaiserslautern, Germany. ²Lehrstuhl Modellierung und Numerik, Universität Trier, Trier, Germany.

Endnotes

^a For details on the commercial software MATLAB we refer to <http://www.mathworks.com>.

^b For details on the commercial software ANSYS Fluent, its models and solvers we refer to <http://www.ansys.com>.

Publisher's Note

Springer Nature remains neutral with regard to jurisdictional claims in published maps and institutional affiliations.

Received: 25 October 2019 Accepted: 25 March 2020 Published online: 02 April 2020

References

1. Arne W, Marheineke N, Pérez-Saborid M, Rivero-Rodriguez J, Wegener R, Wieland M. Whipping of electrified visco-capillary jets in airflows. *SIAM J Appl Math.* 2018;78(1):343–71.
2. Arne W, Marheineke N, Schnebele J, Wegener R. Fluid-fiber-interactions in rotational spinning process of glass wool production. *J Math Ind.* 2011;1(2):1.
3. Arpacı VS. Conduction heat transfer. Pearson Custom Pub; 1991.
4. Brazinsky I, Williams AG, LaNieve HL. The dry spinning process: comparison of theory with experiment. *Polym Eng Sci.* 1975;15(12):834–41.
5. Cibis TM, Leithäuser C, Marheineke N, Wegener R. Homogenization strategies for fiber curtains and bundles in air flows. In: Russo G, Capasso V, Nicosia G, Romano V, editors. *Progress in industrial mathematics at ECMI.* vol. 2014. Berlin: Springer; 2017. p. 971–8.
6. Cibis TM, Marheineke N, Wegener R. Asymptotic modeling framework for fiber-flow interactions in a two-way coupling. In: Fontes M, Günther M, Marheineke N, editors. *Progress in industrial mathematics at ECMI.* vol. 2012. Berlin: Springer; 2014. p. 109–17.
7. Cole KD, Beck JV, Haji-Sheikh A, Litkouhi B. Heat conduction using Green's functions. *Series in computational methods and physical processes in mechanics and thermal sciences.* 2nd ed. Boca Raton: CRC Press; 2010.
8. Gou Z, McHugh AJ. A comparison of Newtonian and viscoelastic constitutive models for dry spinning of polymer fibers. *J Appl Polym Sci.* 2003;87:2136–45.
9. Gou Z, McHugh AJ. Two-dimensional modeling of dry spinning of polymer fibers. *J Non-Newton Fluid Mech.* 2004;118(2–3):121–36.
10. Hairer E, Nørsett SP, Wanner G. Solving ordinary differential equations I, nonstiff problems. 2nd ed. Berlin: Springer; 2009.
11. Manninen M, Taivassalo V. On the mixture model for multiphase flow. *VTT Publ.* 1996;288:1–67.
12. Marheineke N, Wegener R. Modeling and application of a stochastic drag for fibers in turbulent flows. *Int J Multiph Flow.* 2011;37:136–48.
13. Nigmatulin RI. *Dynamics of multiphase media: volume I.* Boca Raton: CRC Press; 1990.
14. Ohzawa Y, Nagano Y. Studies on dry spinning. I. Fundamental equations. *J Appl Polym Sci.* 1969;13:257–83.
15. Ohzawa Y, Nagano Y. Studies on dry spinning. II. Numerical solutions for some polymer–solvent systems based on the assumption that drying is controlled by boundary-layer mass transfer. *J Appl Polym Sci.* 1970;14(7):1879–99.
16. Özisik MN. *Boundary value problems of heat conduction.* Dover books on engineering; 2013.
17. Sano Y. Drying behavior of acetate filament in dry spinning. *Dry Technol.* 2001;19(7):1335–59.
18. Wieland M, Arne W, Feßler R, Marheineke N, Wegener R. Product integration method for simulation of radial effects in dry spinning processes. *Proc Appl Math Mech.* 2018;18:e201800055.
19. Wieland M, Arne W, Feßler R, Marheineke N, Wegener R. An efficient numerical framework for fiber spinning scenarios with evaporation effects in airflows. *J Comput Phys.* 2019;384:326–48.
20. Wieland M, Arne W, Marheineke N, Wegener R. Modeling and simulation of curved fibers in dry spinning scenarios. *Res Appl Math.* 2019. <https://doi.org/10.1016/j.rinam.2019.100013>.
21. Ziabicki A. *Fundamentals of fibre formation.* New York: Wiley; 1976.

Submit your manuscript to a SpringerOpen® journal and benefit from:

- Convenient online submission
- Rigorous peer review
- Open access: articles freely available online
- High visibility within the field
- Retaining the copyright to your article

Submit your next manuscript at ► [springeropen.com](https://www.springeropen.com)